Engineered Science
DOI: https://dx.doi.org/10.30919/es1648

Revealing Soil Mechanics via Coupled Discrete and Finite Element Method Triaxial Testing

Olzhas Sayakov,[1,*] Michael Yong Zhao,[1] Minh Nguyen,[2] Ainash Shabdirova,[1] Kamila Batkuldinova,[1] Bakhtiyar Kalzhan,[1] Sonny Irawan[1] and Dongming Wei[1]

Abstract

This study presents a comprehensive investigation into the mechanical behavior of granular soils through a combined experimental and computational approach using triaxial testing and a coupled Discrete Element Method–Finite Element Method (DEM-FEM) framework. By integrating laboratory experiments with advanced numerical simulations, the research aims to enhance the realism and accuracy of soil behavior modeling under varying stress conditions. The use of flexible membrane modeling, realistic contact laws, and a coarse-graining strategy allows for detailed exploration of particle-level interactions and their influence on macroscopic deformation. Three coarse-graining coefficients (CGC = 3, 6, and 12) were evaluated to assess the trade-offs between computational cost and accuracy. The findings reveal that while higher CGC values improve efficiency, they introduce numerical artifacts, whereas lower CGC values deliver better alignment with experimental results at greater computational expense. CGC = 6 emerges as the optimal compromise, maintaining strong agreement with experimental stress-strain and volumetric responses across multiple confining pressures. The study also confirms that normalized stress-strain relationships are preserved across scales, validating the robustness of the DEM-FEM framework. Overall, this research offers a valuable methodology for bridging micro- and macro-scale mechanics in computational geotechnics and provides guidance on optimizing model resolution for practical engineering applications.

Keywords: DEM-FEM coupling; Coarse-graining; Granular materials; Soil mechanics; Computational geotechnics.
Received: 22 April 2025; Revised: 04 July 2025; Accepted: 04 July 2025
Article type: Research article.

1. Introduction

The mechanical behavior of granular materials, particularly soils, is fundamental to geotechnical engineering, influencing the design and construction of civil infrastructure. Triaxial testing, a cornerstone technique in this field, provides critical insights into soil stability, strength, and deformation under controlled stress conditions.[1,2] This experimental method has been pivotal in evaluating material behavior, offering essential data for understanding soil responses to varied loading environments, which is crucial for safe and effective engineering practices.[3,4,5]

Consolidated drained (CD) triaxial tests are a cornerstone for characterizing the strength, deformation, and failure behavior of granular soils (*e.g.*, sands and gravels) under drained loading. Experiments showed that loose and dense sand specimens converge to the same void ratio at large strains, defining a "critical void ratio" that separates dilative from contractive behavior.[6,7] This discovery laid the foundation for critical state soil mechanics (CSSM), which postulates a unique ultimate state. Later studies confirmed that the friction angle at critical state is governed by mineralogy (around 33° for quartz sands) and that dense sands mobilize higher peak strength due to dilation. (controlled by relative density and confining stress)[8] Bolton's formulation quantified this strength–dilatancy relationship, linking extra shear resistance in dense samples to their tendency to dilate.

Experiments with varying stress histories show that over consolidation increases sand stiffness and accelerates dilation onset, yielding a higher peak shear resistance.[9] Nonetheless, drained triaxial tests demonstrate that irrespective of initial density or preloading, sand accumulates shear strain until reaching the same critical state void ratio.[10,11]

Classical interpretations of triaxial results assume uniform deformation, yet real specimens often develop localized shear bands at failure. Such strain localization violates continuum assumptions and complicates constitutive model calibration.[12] Moreover, inherent fabric anisotropy can make soil strength dependent on loading direction, which basic isotropic models

[1]*Nazarbayev University, 53 Kabanbay batyr Ave., Astana, 010017, Kazakhstan*
[2]*Fulbright University Vietnam, 105 Ton Dat Tien, Hochiminh, 700000, Vietnam*
[*]*Email:* olzhas.sayakov@nu.edu.kz (O. Sayakov)

cannot capture. These complexities have prompted advanced modeling approaches such as nonlocal continuum formulations to handle shear banding and anisotropic critical-state models that include fabric orientation. Discrete-element simulations are increasingly coupled with CD triaxial insights to better capture granular behavior beyond classical frameworks.[13]

Table 1: Dimensions and Physical Properties of the Experimental Sand Specimen.

Property	Value
Height (mm)	75.58
Diameter (mm)	37.24
Membrane thickness (mm)	0.45
Volume (cm^3)	82.280
Mass (g)	145.247
Particle density (g/cm^3)	2.62
Voids ratio	0.4456
Porosity	0.3083

Laboratory triaxial tests enclose the soil specimen in a thin latex membrane to allow free deformation under controlled confinement. Similarly, numerical studies have shown that boundary conditions strongly influence simulated behavior.[14] Rigid lateral boundaries, while convenient for applying pressure, can inhibit the specimen's natural failure processes and deformations.[14] Such rigid walls permit only uniform lateral strain, preventing the local bulging ("barreling") that real specimens exhibit.[15] This lack of deformability suppresses dilation and hinders the onset of strain localization (shear bands), often leading to an overestimation of strength or other discrepancies.[15] Moreover, simply applying confining stress without an actual membrane means that particle–boundary interactions are neglected.[14] The membrane in a physical test transmits pressure through direct contact with grains; without modeling this flexible interface, the simulation cannot capture how particles press into and deform the boundary, affecting force chains and failure patterns. To address these issues, researchers have incorporated flexible membrane models in Discrete Element Methods (DEM), ranging from bonded-particle membranes to coupled continuum meshes, to better replicate the latex membrane's behavior.[14,16] These approaches allow realistic radial deformation and particle–membrane interaction, yielding responses closer to experimental observations. For instance, Qu *et al*. developed a strain energy-based DEM membrane calibrated to latex properties and validated it against lab tests. They found that while the overall stress–strain curve was similar, the flexible boundary had a significant impact on volumetric dilation, bulging failure modes, and internal force networks, compared to a rigid wall .[17] Likewise, recent simulations with flexible Finite Element Methods (FEM) membrane with DEM particles report more pronounced shear band formation, fabric anisotropy evolution, and realistic post-peak softening, aligning much better with experimental data than rigid or periodic boundaries.[18] Notably, using a flexible membrane improves the match to measured stress–strain behavior – reducing errors in peak strength and stiffness – versus rigid-wall simulations.[15] Researchers caution that the membrane's properties must be chosen carefully, as an overly stiff or coarse membrane can impose extra confinement on the sample.[19] Overall, the literature suggests that modeling a deformable membrane is crucial for capturing the true deformation mechanisms (dilation, bulging and strain localization) in granular media. This motivates the present use of a coupled DEM–FEM approach with a realistic flexible membrane, in order to faithfully simulate particle–membrane interactions and improve the predictive accuracy of triaxial test models.

Coupling DEM with FEM leverages the strengths of each to model granular soils more realistically. DEM represents grain-scale physics (contact friction, dilation, particle rearrangements) that continuum models often idealize, while FEM efficiently handles large-scale boundaries and continuum regions.[20] Rather than choose one method, modern 3D DEM–FEM frameworks use both "for what they are good at," replacing phenomenological constitutive laws with a DEM-based micro-mechanical response inside an FEM macro-scale model. This integration naturally bridges micro- and macro-mechanics: the granular assembly's emergent behavior informs the continuum response, and vice versa. As a result, coupled models capture complex phenomena like strain localization and shear banding that DEM reproduces at the grain scale (shear band thickness relates to grain size), without sacrificing the scale and flexibility advantages of FEM.

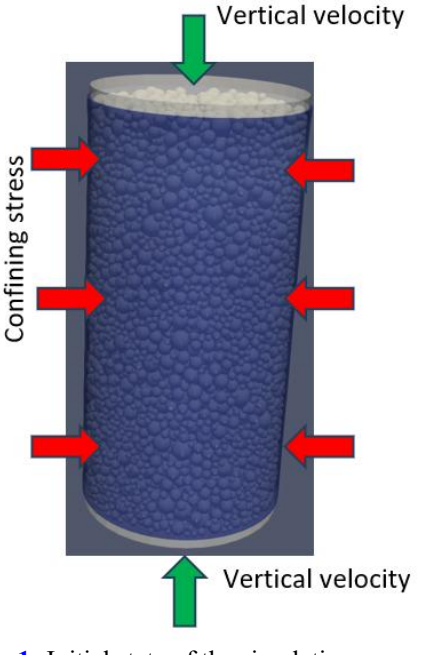

Fig. 1: Initial state of the simulation process.

In triaxial test simulations, DEM–FEM coupling has clear benefits. For example, a flexible rubber membrane can be modeled with FEM while sand or gravel particles are

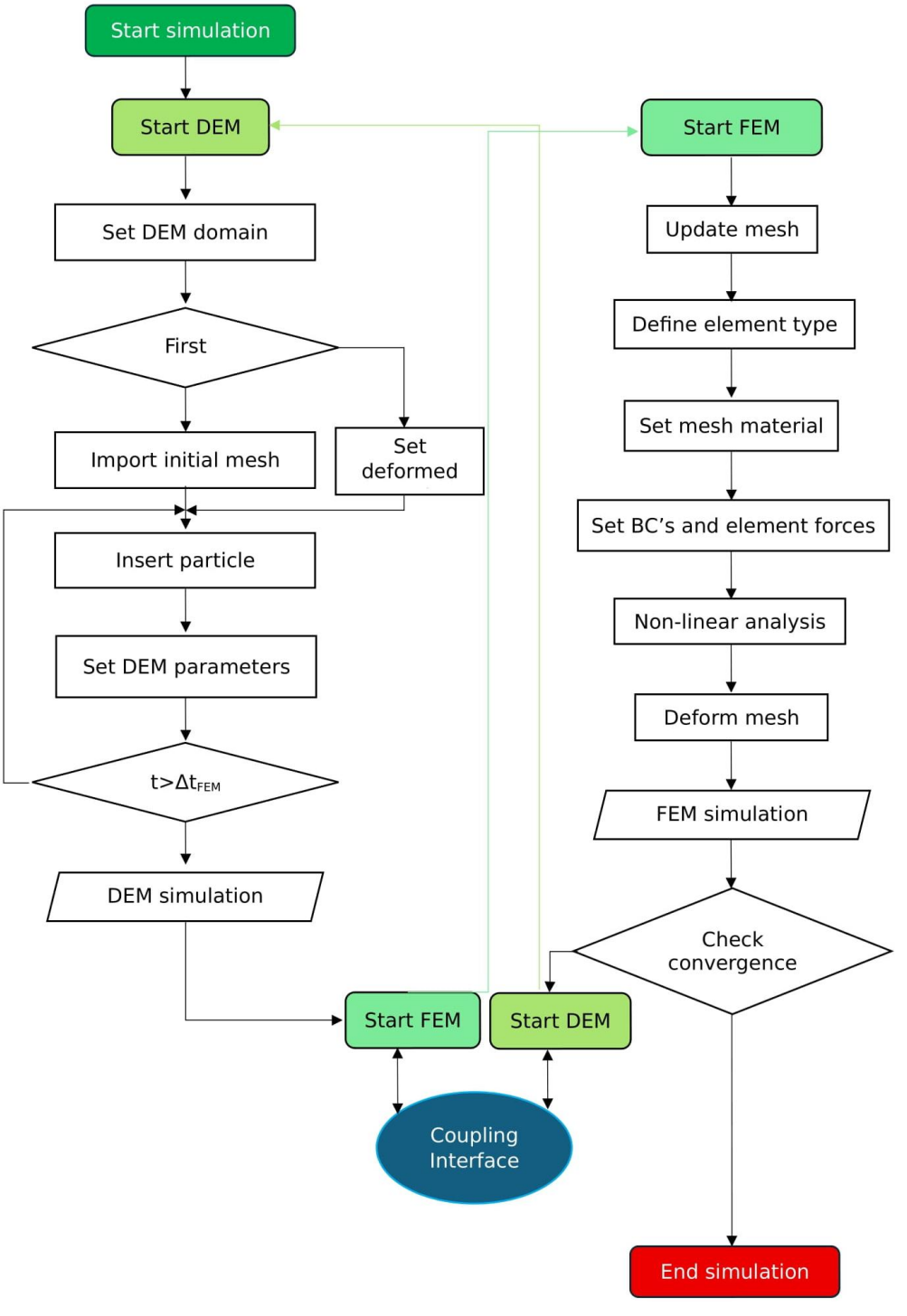

Fig. 2: Schematic representation of the DEM-FEM coupling.

simulated with DEM.[21] This allows realistic particle–boundary interactions: each grain's contact force on the membrane is mapped into the FEM as a distributed traction, causing the membrane to deform and apply back-pressure on the particles.[22] Such two-way force mapping reproduces confining pressure effects and sample deformation more faithfully than rigid or particle-based boundaries. Using a proper contact model (*e.g.* nonlinear Hertz–Mindlin law) for grain–grain and grain–wall contacts further improves realism, capturing elastic-frictional contact behavior.[23,24] To ensure accuracy, micro-parameters (particle stiffness, friction, etc.) are calibrated so that the DEM assembly's stress–strain response matches lab data, and the FEM membrane's material is tuned to mimic a latex enclosure. Studies confirm that DEM–FEM models can tackle complex soil behavior (*e.g.* particle breakage under high pressure) beyond the reach of DEM-only or FEM-only approaches.[25] By uniting grain-scale detail with continuum-scale context, the DEM–FEM approach

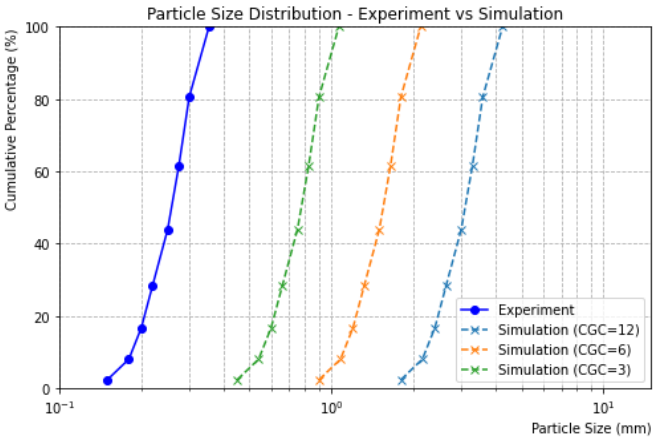

Fig. 3: Particle Size Distribution (PSD) – Comparison Between Experiment and Simulation for Different Coarse-Graining Coefficients.

provides a more predictive and insightful tool for simulating realistic triaxial behavior of granular materials.Coarse-graining (CG) techniques in DEM and DEM-FEM simulations offer a practical trade-off between computational cost and mechanical fidelity for granular materials. Instead of modeling every grain, groups of particles are replaced by a larger "super-particle," reducing particle count dramatically.[26,27] This approach can yield order-of-magnitude speed-ups – for example, a recent study achieved about nine times faster simulations using coarse-grained parcels while still matching the original model's sand production rates and velocity profiles.[28] Proper scaling laws are crucial when increasing particle size so that bulk behavior (*e.g.* mass, contact stiffness, and energy dissipation) remains consistent with the fine-grained system.[27] Studies have established rules to adjust particle density and contact parameters for enlarged grains, preserving volume fraction and mechanical response.[26] Indeed, when exact scaling laws are applied, the coarse-grained model can closely reproduce the original system's behavior, although some loss of precision is inevitable as the scale factor grows.[27]

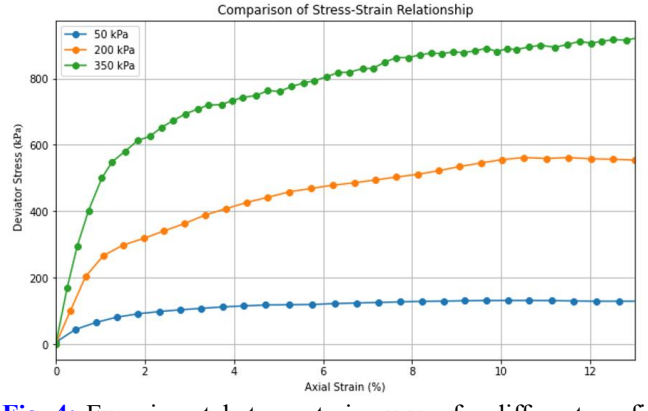

Fig. 4: Experimental stress-strain curves for different confining pressures.

Different coarse-graining coefficients (CGC) have been tested to find an optimal balance. Increasing CGC greatly reduces computational cost but tends to degrade accuracy – errors in macro-scale stress or deformation responses grow as CGC increases.[27] At very high CGC, issues such as boundary distortion and an underestimation of contact interactions can emerge, since fewer, larger particles cannot capture fine contact network details.[29] To mitigate these effects, multi-scale approaches have been proposed. For instance, Queteschiner *et al.* introduced multi-level CG, embedding fine-grained regions near boundaries within coarse domains to improve fidelity.[29] Overall, prior research indicates that a moderate coarse-graining factor (~4–6) provides the best compromise between efficiency and accuracy.[26,27] In light of these findings, using CGC = 6 is often recommended as an optimal choice – it substantially lowers computation time while maintaining bulk mechanical behavior within acceptable error bounds.[26,28] This balance has been validated by experiments and simulations, which show that CGC = 6 retains realistic stress–strain and flow characteristics of granular assemblies, whereas higher ratios lead to pronounced deviations.[26] Such consensus in the literature underpins the selection of CGC = 6 for the present work as a viable trade-off between computational feasibility and mechanical realism.

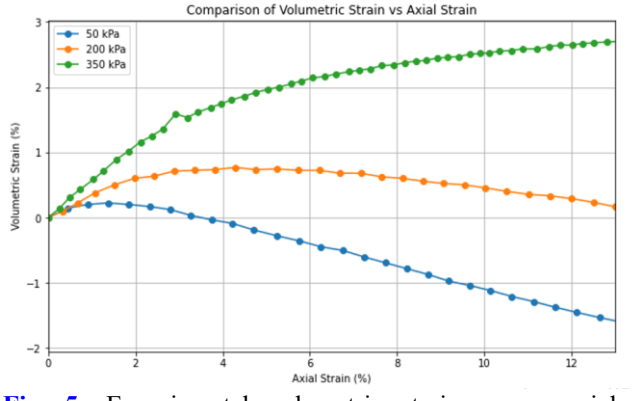

Fig. 5: Experimental volumetric strain versus axial strain behavior for different confining pressures.

Despite the significant advancements in triaxial testing and DEM-FEM simulations, challenges remain in accurately modeling particle-membrane interactions and capturing nuanced soil behaviors under complex stress conditions. Simplified boundary conditions and contact laws often fail to represent the dynamic interactions within granular materials, limiting the predictive accuracy of simulations.

This study aims to address these gaps by integrating advanced contact models and flexible membrane simulations within a DEM-FEM framework. By incorporating more realistic particle-membrane interactions and enhancing computational efficiency through coarse-graining techniques, this research seeks to improve the predictive capabilities of triaxial testing simulations, contributing to safer and more efficient geotechnical engineering practices. This coupled approach has broad applications across civil, mining, aerospace, and petroleum engineering. For example, it has been used to simulate soil-geogrid interlocking, seismic

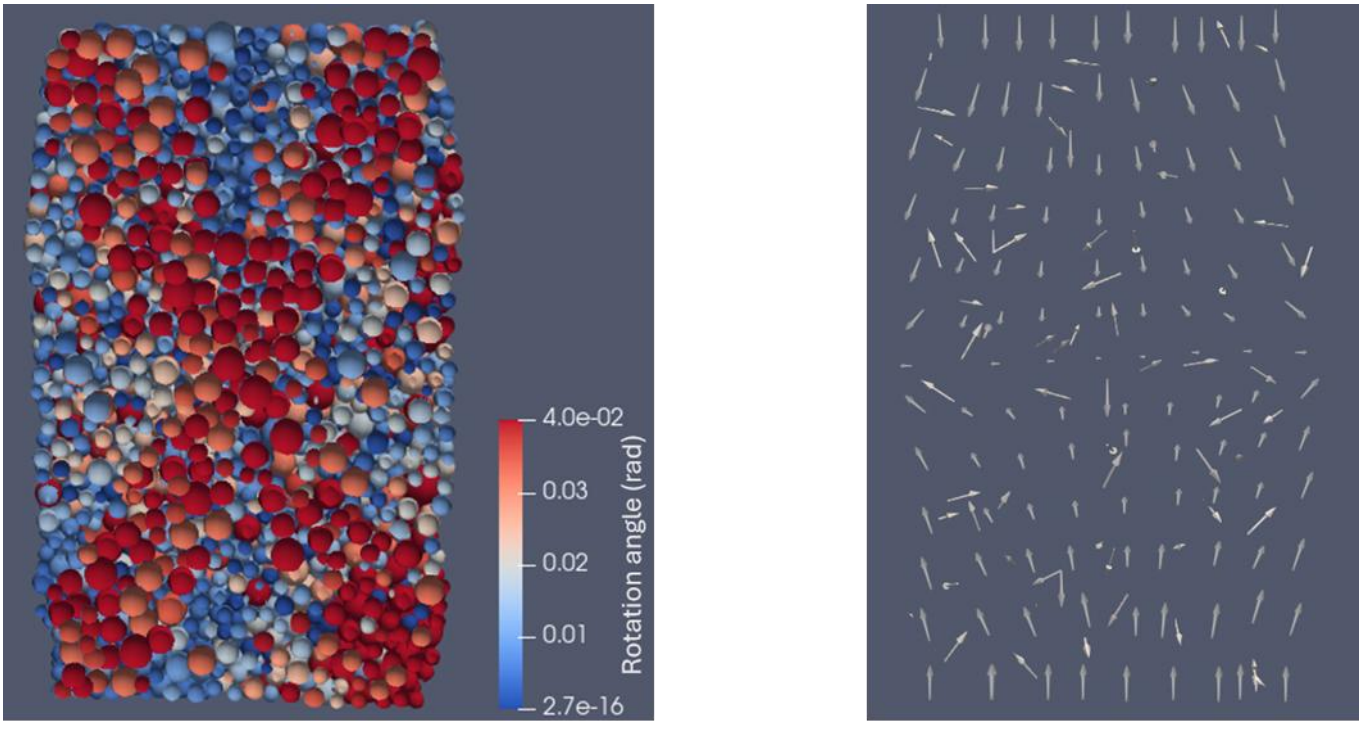

Fig. 6: Micromechanical localization at 10 % strain. (a) Rotation map reveals a 60° shear band. (b) Displacement vectors diverge along the same plane, confirming the band.

responses of embankments, and interactions in hydraulic fracturing, as well as to investigate particle breakage in granular soils under high confining pressure, model hypervelocity impacts on spacecraft debris shields, and analyze the uplift behavior and failure mechanisms of suction buckets embedded in granular soil.[30,31,32] Recent research has also highlighted the transformative potential of incorporating contact models, such as the Hertz-Mindlin (HM) models, which provide more realistic depictions of particle-level interactions and elastic-plastic deformation transitions.[33,34]

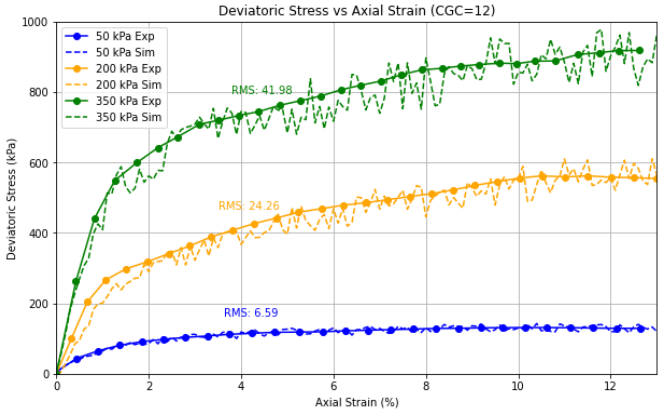

Fig. 7: Comparison of experimental and simulated deviatoric stress vs axial strain for CGC = 12.

Moreover, the scope of triaxial testing has evolved with the integration of sustainable materials and innovative modeling techniques. Applications such as microbial-induced carbonate precipitation (MICP) and biochar have advanced sustainable geotechnical solutions, demonstrating the adaptability of triaxial testing to address modern engineering challenges.[35,36] Additionally, the use of flexible membranes in DEM-FEM simulations has improved the accuracy of modeling soil and rock behavior by capturing shear band formation, pore pressure evolution, and stress heterogeneity in granular materials, as well as replicating brittle-ductile transitions in rock samples under triaxial compression.[37,38]

Despite these advancements, challenges remain in accurately modeling the complex interactions within granular materials. Many existing models rely on rigid boundaries or simplified contact laws, which fail to capture the nuanced behaviors of soils under realistic conditions. This study seeks to address these limitations by integrating advanced contact models and flexible membrane simulations within a DEM-FEM framework. The aim is to improve the predictive capabilities of these simulations, making them more reflective of real-world soil responses under triaxial testing conditions.

Although coupled Discrete Element Method–Finite Element Method (DEM–FEM) frameworks have been applied to triaxial testing before, the present study advances the technique by uniting three key innovations in a single, rigorously validated pipeline: (i) a deformable latex-like membrane modeled with FEM that exchanges forces bidirectionally with DEM particles at every timestep, faithfully capturing particle–boundary interactions often overlooked in earlier rigid-wall studies; (ii) a systematic coarse-graining protocol that quantifies the trade-off between computational cost and stress–strain fidelity across three

scaling factors (CGC = 3, 6, 12), thereby offering clear guidance on model resolution for practical engineering use; and (iii) calibrated Hertz-Mindlin contact laws and force-mapping algorithms that reproduce micromechanical phenomena—shear-band localization, force-chain evolution, and dilation—consistently with laboratory data. Together, these elements transform an otherwise traditional DEM–FEM setup into a micro-to-macro simulation framework that delivers both high accuracy and computational efficiency, providing a demonstrable step beyond conventional triaxial-test modeling approaches.

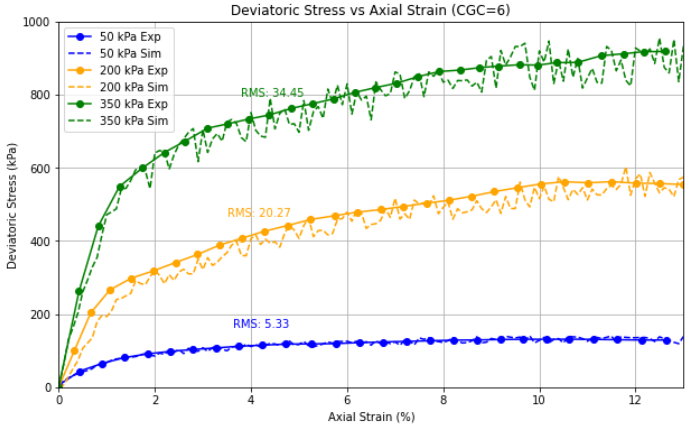

Fig. 8: Comparison of experimental and simulated deviatoric stress vs axial strain for CGC = 6.

In this research, the focus is on enhancing the accuracy and applicability of DEM-FEM simulations by:

1. Incorporating advanced contact models that simulate elastic and plastic deformation behaviors more precisely.
2. Integrating flexible membranes that adapt to natural soil deformations, providing a more realistic representation of stress states.
3. Leveraging a coupled DEM-FEM framework to ensure seamless transmission of forces and deformations across the soil sample.

By addressing these objectives, this study aims to contribute significantly to the field of geotechnical engineering, offering a robust framework for understanding soil behavior under complex loading conditions and facilitating the design of safer and more efficient infrastructure. The findings are expected to advance the state of the art in triaxial testing and computational modeling, paving the way for innovative geotechnical solutions.

2. Methods

2.1 Experimental design

Drained triaxial compression tests, conducted in accordance with ASTM D7181 and D4767, provided the experimental benchmarks for this study. A cylindrical sand specimen (height ≈ 75 mm, diameter ≈ 37 mm) taken from a cleaned reservoir core was encased in a latex membrane and mounted in a water-pressurised triaxial cell (Fig. S1). Key geometric and physical properties—including membrane thickness, bulk density, porosity and void ratio—are summarised in Table 1. After saturation to a B-value ≥ 0.96, the specimen was isotropically consolidated under effective confining stresses of 50, 200 and 350 kPa, then sheared at a constant axial-strain rate of 0.05 mm min^{-1} while drainage was maintained. Axial load, axial displacement (±0.001 mm via external LVDTs) and specimen volume change (±0.01 cm^3 via a burette system) were recorded continuously to produce deviatoric stress–strain and volumetric strain–axial strain curves that serve as quantitative reference data for validating the coupled DEM–FEM simulations.

2.2 Simulation framework

This study utilizes a coupled DEM-FEM approach to simulate the mechanical behavior of granular materials confined within a flexible membrane, as observed in triaxial compression tests (see Fig. 1). The DEM solver, Aspherix®, models the granular particles, capturing their individual and collective interactions. The FEM solver, Elmer, represents the flexible membrane, allowing for the analysis of its deformation in response to particle-induced forces. This coupling enables a detailed examination of the interactions between the granular assembly and its confining boundary, providing insights into the material's macroscopic behavior under load.

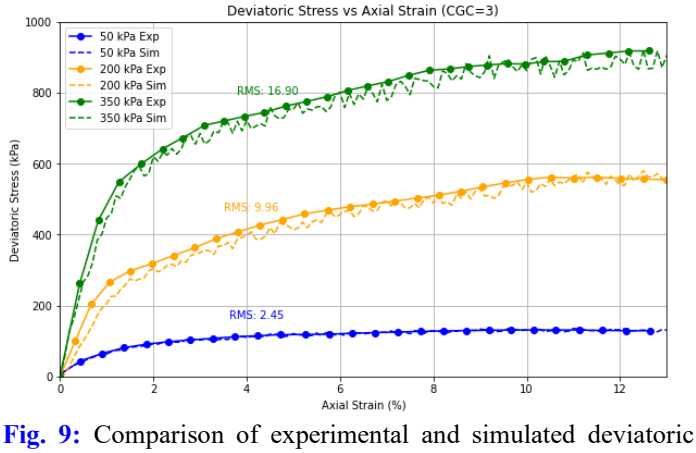

Fig. 9: Comparison of experimental and simulated deviatoric stress vs axial strain for CGC = 3.

2.3 DEM-FEM coupling

The integration of Aspherix® and Elmer is achieved through a co-simulation strategy that enables dynamic information exchange between the DEM and FEM solvers at each simulation timestep. Fig. 2 illustrates the schematic representation of the DEM-FEM coupling, detailing the iterative process between the two solvers for accurate simulation. The coupling begins with the DEM computation, where Aspherix® calculates the contact forces acting between particles as well as between particles and the flexible membrane. These interaction forces, particularly those exerted on the membrane surface, are identified and prepared for

transfer to the FEM solver.

Once computed, the contact forces from Aspherix® are mapped onto the corresponding nodes or finite elements of the membrane model within Elmer. This force mapping ensures that the membrane's structural response to localized particle interactions is accurately captured by the FEM solver. Elmer then proceeds to compute the resulting deformation of the membrane under these applied loads, updating the nodal displacements and internal stresses accordingly.

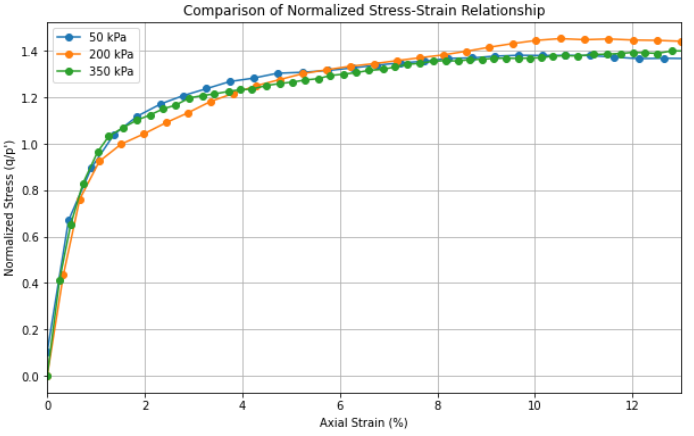

Fig. 10: Normalized experimental stress-strain curves for 50 kPa, 200 kPa, and 350 kPa.

Following the FEM computation, the updated displacement data of the membrane is communicated back to Aspherix®. The DEM solver uses this information to adjust the positions and boundary conditions of the particles that interact with the deformed membrane, ensuring consistency in the particle-environment interactions.

This coupled process iterates within each timestep, and convergence is assessed by monitoring the changes in forces and displacements exchanged between the solvers. Once these changes fall below a predefined threshold, convergence is considered achieved. Through this iterative and synchronized exchange, the simulation accurately captures the complex interactions between the granular particles and the deformable membrane, maintaining numerical stability and physical realism throughout the simulation.

2.3.1 Contact models

1. Particle-Particle Interactions: The Hertz-Mindlin contact law was used to simulate normal force Eq. (1) and tangential force Eq. (4) between particles when their distance r is less than their contact distance $d = r_i + r_j$. Normal force:

$$F_n = k_n \delta_n - \gamma_n v_n \quad (1)$$

- k_n is the normal stiffness as shown in Eq. (2).
- $\delta_n = d - r$ is the overlap.
- γ_n is the damping constant as shown in Eq. (3).
- v_n is the relative normal velocity.

The normal stiffness k_n is given by:

$$k_n = \frac{4}{3} Y^* \sqrt{r * \delta_n} \quad (2)$$

- Y^* and r^* are equivalent material properties based on Young's modulus and Poisson's ratio of the interacting particles.

The damping constant is:

$$\gamma_n = 2\sqrt{\frac{5}{6}} \beta \sqrt{S_n m^*} \quad (3)$$

where $S_n = 2Y^*\sqrt{r^*\delta_n}$ and β is a function of the coefficient of restitution e.

Similarly, the tangential contact force is defined as:

$$F_t = k_t \delta_t - \gamma_t v_t \quad (4)$$

- k_t and γ_t denote the tangential stiffness and damping coefficients as in Eq. (5) and (6), respectively.
- δ_t is the accumulated tangential displacement.
- v_t is the relative tangential velocity at the contact interface.

The normal stiffness k_n is given by:

$$k_t = 8G^* \sqrt{r * \delta_n} \quad (5)$$

- $G^*$is the equivalent shear modulus.

The tangential damping coefficient is expressed as:

$$\gamma_t = 2\sqrt{\frac{5}{6}} \beta \sqrt{S_t m^*} \quad (6)$$

- where $S_t = 8G^*\sqrt{r^*\delta_n}$.

For scenarios requiring more physically accurate modeling, especially under varying normal loads, Aspherix® supports the Hertz–Mindlin model, a nonlinear formulation that captures the deformation-dependent nature of contact stiffness. This model considers the geometric and material properties of the particles and provides more reliable predictions for dynamic systems and dense particle assemblies. The choice between these models depends on the specific characteristics of the granular material and the objectives of the simulation.

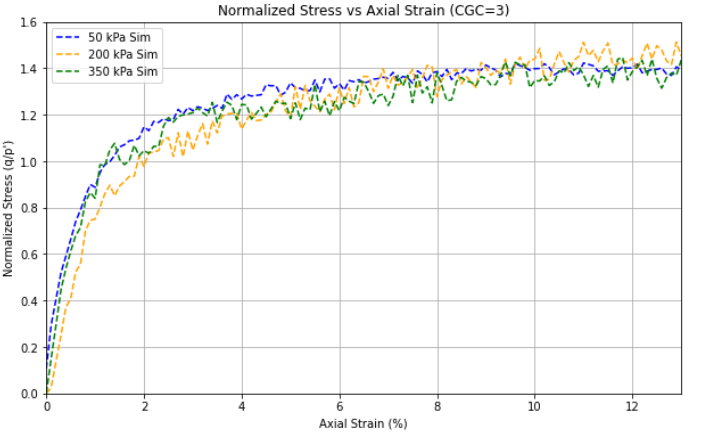

Fig. 11: Comparison of normalized simulated stress-strain responses (CGC = 3) across different confining pressures.

Table 2: Comparison of Experimental and Simulated Parameters for Different Coarse-Graining Coefficients.

Parameter	Experiment	Simulation (CGC=12)	Simulation (CGC=6)	Simulation (CGC=3)
Young's modulus (Pa)	70e9	2250e9	915e9	125e9
Friction coefficient	0.35	4.5	2.8	1.3
Simulation time (hours)	16	32	66	135
Number of particles		8500	71600	622400

The linear model offers simplicity and computational efficiency, while the Hertz–Mindlin model introduces greater realism at the cost of increased computational demand. These mechanics are visually illustrated in Supplementary Fig. S2, which shows two particles in contact, highlighting the direction of normal and tangential forces, the overlap between particles, and the associated relative velocities.

2. Flexible Membrane Model: The flexible membrane is modeled using FEM, where the stress-strain relationship is used to describe the deformation behavior. For small deformations, the strain-displacement relationship is expressed as in Eq. (7).

$$\epsilon = Bu \tag{7}$$

- ϵ is the strain.
- B is the strain-displacement matrix.
- u is the displacement vector.

Although the model applies a small deformation assumption, the membrane is allowed to undergo noticeable displacement during loading, which may exceed the limits of linear strain theory in some cases. Nodal displacements resulting from contact forces between particles and the membrane are resolved at each timestep and are essential for maintaining realistic boundary conditions. Accurate modeling of this deformation within the DEM-FEM framework is critical for representing particle-boundary interactions and ensuring reliable simulation results.

The stress is calculated as in Eq. (8).

$$\sigma = D\epsilon \tag{8}$$

where D is the material stiffness matrix, based on the Young's modulus and Poisson's ratio of the membrane material.

3. Particle–Membrane Interactions: In the coupled DEM–FEM framework, particle–membrane contact forces are detected and computed by Aspherix®, then transferred to Elmer, which returns the corresponding membrane deformation; the force–mapping sequence is illustrated in Supplementary Fig. S3.

a. When a particle approaches and penetrates the membrane surface (modeled by finite elements), a contact is registered. Similar to particle–particle contact, a spring-dashpot model or a Hertzian formulation is applied to compute the interaction force.

i. Normal contact force:

$$F_n^{pm} = k_n^{pm}\delta_n^{pm} - \gamma_n^{pm}v_n^{pm} \tag{9}$$

- k_n^{pm} is the normal stiffness between the particle and membrane.
- δ_n^{pm} is the overlap between the particle and membrane.
- γ_n^{pm} is the damping constant between the particle and membrane.
- v_n^{pm} is the normal component of relative velocity at the contact point.

ii. Tangential contact force:

$$F_t^{pm} = k_t^{pm}\delta_t^{pm} - \gamma_t^{pm}v_t^{pm} \tag{10}$$

- k_t^{pm} and γ_n^{pm} are tangential stiffness and damping parameters respectively.
- δ_t^{pm} is the tangential displacement accumulated at the contact interface.
- v_t^{pm} is the relative tangential velocity.

b. Force Mapping to FEM Mesh:

The contact forces computed by Aspherix® are not applied at a single point but are distributed over the nodes of the impacted FEM elements in Elmer. This ensures equilibrium and compatibility of forces at the contact surface, smoother deformation of the membrane and physically accurate feedback to the DEM solver. Elmer receives these nodal forces and updates the membrane deformation, which is then interpolated back to the DEM as updated particle boundary constraints.

c. Coupling Considerations:

- Contact stiffness k_n^{pm} is often calibrated based on experimental data or derived from contact mechanics.
- Penetration depth is kept small to maintain numerical stability and realism.
- Time integration schemes in Aspherix® (typically explicit) are matched in resolution with the FEM solver's timestep to avoid instability in the exchange.

2.3.2 Coarse graining approach

The particle size distribution (PSD) in the numerical model was designed to closely match the experimental PSD obtained from real granular soil samples. A polydisperse particle size distribution was implemented to reflect the natural heterogeneity of the material. The experimental PSD and its numerical representation for different CGCs are compared in Fig. 3.

To achieve a computationally feasible simulation, a coarse-graining strategy was employed. With the real particle sizes, the total number of particles required for an accurate numerical representation would be approximately 13500000, which is computationally impractical.

To reduce the computational burden while maintaining mechanical consistency, CGC of 3, 6, and 12 were evaluated. Increasing CGC results in a shift toward larger particle diameters, modifying the PSD compared to the experimental distribution. The number of simulated particles was reduced to 622400 for CGC = 3, 71600 for CGC = 6, and 8500 for CGC = 12, significantly lowering computational costs.

Scaling laws ensured mechanical consistency between coarse-grained particles and real granular materials. Parameters, including the friction coefficient and Young's modulus, were calibrated through systematic calibration tests, comparing numerical and experimental stress-strain behaviors to minimize deviations. Table 2 summarizes these parameters and illustrates the trade-offs between accuracy and computational efficiency for each CGC. The differences in parameters between simulations and experimental values reflect adjustments needed to maintain accurate mechanical responses under various coarse-grained resolutions, as determined from calibration analyses.

2.3.3 Computational implementation and solver details

Simulations were performed using Aspherix®, a comprehensive DEM software developed by DCS Computing GmbH. Aspherix® offers advanced capabilities for simulating complex particle systems and built-in coupling interfaces for seamless integration with FEM analyses. The DEM-FEM coupling within Aspherix® allowed efficient force and displacement data exchange.

The computational setup consisted of a high-performance workstation with two Intel Xeon E5-2699 v4 processors (22 cores, 44 threads each), totaling 88 threads. The system included 503 GiB RAM and GPU acceleration provided by an NVIDIA Quadro P6000 (24 GB VRAM), ensuring numerical stability and efficiency during intensive computations.

Simulation timesteps were set to 10^{-9} s (DEM) and 10^{-7} s (FEM), ensuring precise force-displacement updates. The full set of computational and material parameters used in every run is summarised in Supplementary Table S1, which was validated through calibration tests.

2.3.4 Particle generation and boundary setup

In the DEM-FEM simulations, particles were generated within the triaxial cell using a randomized spatial distribution to replicate the initial density and arrangement observed in the experimental setup. Initially, the particles were generated above the membrane and allowed to fall under gravity into the enclosed space. To achieve the target porosity, the top cap was used to gently compress the particles, ensuring a realistic packing structure before external stresses were applied. Fig. 1 presents the initial state of the simulation process, depicting the particle distribution and boundary setup for the coarse-graining cases.

The boundary conditions were designed to reflect the experimental triaxial test conditions. A confining pressure of 50 kPa, 200 kPa, and 350 kPa was applied through the flexible membrane in different simulation cases, allowing realistic lateral deformation during compression. Axial loading was applied through both the top and bottom caps, which moved at a controlled velocity to replicate the uniform compression process in the physical test. Unlike conventional setups where the bottom boundary is fixed, in this study, it was displaced in coordination with the top cap to ensure proper stress distribution and deformation behavior.

To balance numerical accuracy and computational efficiency, different axial strain velocities were tested in the DEM-FEM simulations. The velocities considered were 0.05 m/s, 0.02 m/s, 0.01 m/s, and 0.005 m/s, with their impact on stress-strain response and volumetric strain behavior carefully evaluated. The relative error was assessed by comparing results between consecutive strain rates. First, the 0.05 m/s case was compared with 0.02 m/s, followed by a comparison between 0.02 m/s and 0.01 m/s, and finally, between 0.01 m/s and 0.005 m/s. This stepwise approach allowed for a progressive refinement of strain rate selection while ensuring that computational costs remained manageable. As shown in Supplementary Table S2, the 0.02 m/s velocity was chosen, as its stress-strain response differed by less than 5% from the 0.01 m/s case, while still significantly reducing computational time compared to lower strain rates. Higher velocities, particularly 0.05 m/s, led to a noticeable increase in relative error, especially in volumetric strain. Since the relative difference between 0.01 m/s and 0.005 m/s was minimal, further reduction in strain rate was deemed unnecessary. The final selection of 0.02 m/s ensured an optimal balance between simulation accuracy and computational efficiency, making it the most suitable strain rate for further numerical analyses.

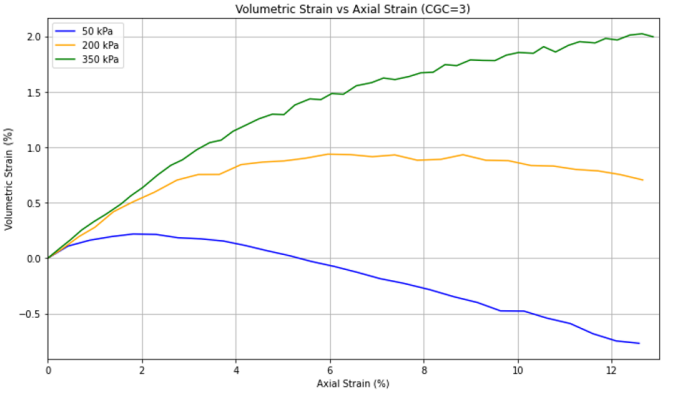

Fig. 12: Simulated volumetric strain vs. axial strain curves for 50, 200, and 350 kPa (CGC = 3).

To accurately model particle-membrane interactions, friction parameters were incorporated based on experimental values. The particle-wall and particle-membrane contact properties were calibrated to ensure that stress transmission and

deformation behavior aligned with physical observations.

To validate the membrane's deformation and internal volume changes during the simulation, a custom Python script was developed. This script processes the VTU/PVTU mesh output from Aspherix®, calculates the internal volume of the flexible membrane, and tracks its evolution over time. Using a Convex Hull approximation, the script ensures an accurate representation of membrane deformation and boundary movement. The computed volume data is exported as a function of time, allowing for direct comparisons with experimental measurements. The full implementation of this script is available in the GitHub repository associated with this study.

2.3.5 Parameter-sensitivity check

To verify that the calibrated inputs were not coincidental, we repeated the 50 kPa simulation at every coarse-graining level and perturbed the two parameters that control macroscopic stiffness and strength, namely the particle Young's modulus and the inter-particle friction coefficient, by roughly ±25 % around their baseline values. All other inputs (membrane properties, cap velocity, damping) were held fixed. After every trial the simulated stress-strain curve was compared with the experimental benchmark and the root-mean-square deviation was recorded. Supplementary Table S3 summarizes the sweep: for CGC = 3, 6 and 12 the RMS error drops steadily to a distinct minimum, and those minima define the parameter sets used in all subsequent simulations. The monotonic trend indicates that the model response is locally well behaved, and that the chosen calibrations lie near a joint optimum rather than an arbitrary point in a flat landscape.

2.3.6 Macroscopic Shear-Band Orientation

For dense granular materials, the inclination β of a shear band with respect to the major principal-stress axis is commonly related to the peak (bulk) friction angle φ by the Coulomb orientation rule,

$$\beta = 45^0 + \frac{\varphi}{2} \tag{11}$$

as given in Eq. (11). The friction angle itself is defined by the shear-to-normal stress ratio acting on the failure plane,

$$\tan\varphi = \frac{\tau}{\sigma_n} \tag{12}$$

shown in Eq. (12). These two expressions are invoked in Section 4.2.2 to translate the simulated shear-band inclination into the experimentally measured peak friction angle and to verify the model's macroscopic strength response.

3. Results

3.1 Experimental observations

3.1.1 Overview of experimental procedure

The experimental study involved conducting a series of CD triaxial tests on a real sand specimen to investigate the mechanical behavior of granular soil under varying confining pressures. The specimen was enclosed in a flexible membrane and subjected to controlled axial loading while maintaining drained conditions to prevent excess pore pressure buildup. Three different confining pressures—50 kPa, 200 kPa, and 350 kPa—were applied to assess their influence on the soil's stress-strain response and volumetric strain behavior.

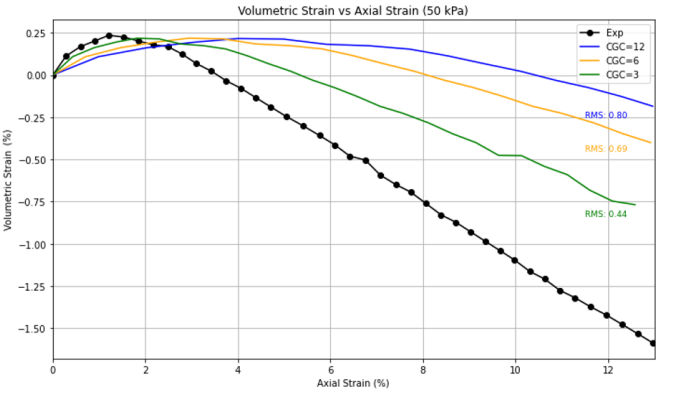

Fig. 13: Comparison of experimental and simulated volumetric strain for 50 kPa at different CGCs.

3.1.2 Final deformed specimen and failure mode

Upon completion of the shearing phase, the sand specimen exhibited a characteristic barrel-shaped deformation, a commonly observed failure mode in granular soils subjected to triaxial compression. The deformation pattern was indicative of strain localization and dilation effects, particularly at higher confining pressures. The extent of lateral bulging is shown in Supplementary Fig. S4.

3.1.3 Experimental stress-strain behavior across different confining pressures

The experimental stress-strain responses for different confining pressures were analyzed to assess the strength characteristics of the sand specimen. Fig. 4 illustrates the deviatoric stress versus axial strain curves for confining pressures of 50 kPa, 200 kPa, and 350 kPa. The results indicate an expected trend where higher confining pressures resulted in greater peak deviatoric stress values, demonstrating increased shear strength due to enhanced particle confinement. The curves also reveal strain-hardening behavior, with the stress reaching a peak before stabilizing at large strains.

3.1.4 Experimental volumetric strain-axial strain behavior

The evolution of volumetric strain during axial loading was also examined to understand the dilative and contractive tendencies of the granular assembly. Fig. 5 presents the volumetric strain versus axial strain curves for the three confining pressures. At lower confining pressures (50 kPa), the specimen exhibited noticeable dilation, characterized by an increase in volume at large axial strains. In contrast, at higher confining pressures (200 kPa and 350 kPa), the material initially showed a contractive response, transitioning into

dilation at later stages of deformation. This behavior aligns with expected trends in dense granular materials, where dilation becomes more pronounced at lower confinement levels.

3.1.5 Key observations from stress-strain and volumetric strain analysis

- The peak deviatoric stress increased with higher confining pressures, confirming the dependency of shear strength on confinement.
- The lower confining pressure case (50 kPa) showed a more distinct dilation phase, while higher confining pressures exhibited an initial contractive phase before transitioning to dilation.
- The stress-strain and volumetric strain responses provide a reference for validating numerical simulations, ensuring that the DEM-FEM models accurately capture the experimental behavior.

These findings serve as a benchmark for evaluating the performance of numerical models, which will be compared in the subsequent sections.

3.2 DEM-FEM simulation results

The DEM-FEM coupled model was designed to replicate the experimental triaxial test conditions, incorporating realistic particle interactions, membrane deformations, and boundary constraints. The DEM component captured the discrete granular interactions, while the FEM model accounted for the deformable membrane, ensuring accurate stress-strain behavior under different confining pressures. The numerical setup carefully mirrored the experimental conditions, including membrane flexibility, applied confining pressures, and controlled axial strain rates.

One of the key considerations in the simulation was computational feasibility. Given the high particle count required for accurate representation, CGC approach was implemented to balance computational cost and mechanical fidelity. Three CGC values were tested (12, 6, and 3), where a higher CGC reduced the number of particles but required appropriate scaling laws to preserve bulk mechanical behavior. Specifically, simulation times varied significantly depending on the chosen CGC: simulations with CGC = 12 required approximately 32 hours, CGC = 6 took 66 hours, and the most detailed simulations with CGC = 3 demanded approximately 135 hours of computational time. The effect of CGC on simulation accuracy was assessed by comparing simulated and experimental stress-strain responses across different confining pressures. This computational analysis underscores the critical balance between simulation fidelity and efficiency, aiding in selecting optimal resolution levels for DEM-FEM simulations in computational geotechnics.

Detailed visualisations of mesh deformation, membrane stresses and internal particle kinematics are provided in Supplementary (Fig. S5–S7). In brief, semi-transparent mesh renderings (Fig. S5) show that the specimen remains uniformly packed at 0 % axial strain, develops pronounced radial bulging and particle re-orientation by 5 %, and displays a well-defined voided shear band at 10 %. The corresponding membrane-stress maps (Fig. S6) reveal a transition from a nearly uniform stress field to a centre-line localisation that tracks the outward barrel shape, confirming realistic boundary interaction. Cross-sectional particle snapshots (Fig. S7) corroborate these trends: grain rearrangement initiates near the membrane, propagates inward with increasing strain, and culminates in a distinct inclined localisation zone that matches the volumetric-dilation onset observed experimentally.

3.2.1 Micromechanical evidence of failure.

Fig. 6 pinpoints the grain-scale process behind macroscopic softening. Fig. 6a displays a rotation-intensity map in which a continuous corridor, roughly 12 d_{50} thick, tilts about 60° from the loading axis. Fig. 6b illustrates particle displacement vectors, corroborating this shear localization: grains within the band exhibit pronounced lateral and upward displacement, while those outside the band show minimal vertical displacement. Each arrow originates at the grain's initial (tail) position and terminates at its current (head) position, and the arrow length is proportional to the displacement magnitude—longer arrows identify grains that have travelled farther. This 60° inclination satisfies the Coulomb orientation criterion given by Eq. (11), which in turn yields a peak friction angle φ of 30–33°, matching the value back-calculated from experimental stress–strain curves (Fig. 4) and consistent with the definition in Eq. (12). Hence, the coupled DEM–FEM model reproduces both the correct shear-band geometry and the bulk frictional strength observed in the laboratory, linking particle-scale rotation and translation to specimen-scale shear resistance and dilation.

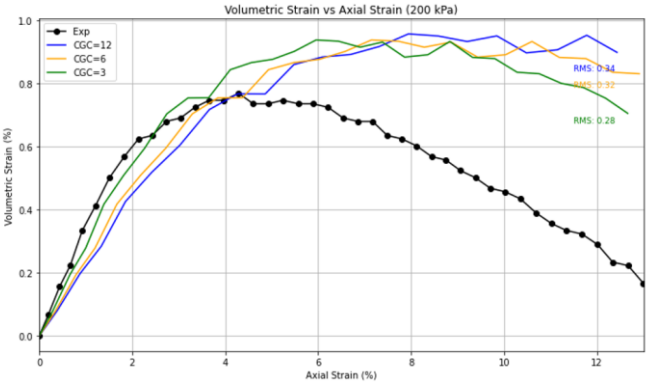

Fig. 14: Comparison of experimental and simulated volumetric strain for 200 kPa at different CGCs.

3.2.4 Deviatoric stress vs axial strain comparison

The comparison between experimental and simulated deviatoric stress vs axial strain curves provides valuable insight into how well the DEM-FEM model reproduces granular soil behavior under different stress conditions. Fig. 7

presents the stress-strain behavior for confining pressures of 50 kPa, 200 kPa, and 350 kPa at CGC = 12. The overall trend of the experimental curves is captured, but fluctuations in the numerical results are evident, particularly around the peak stress. These oscillations are indicative of particle-scale heterogeneities and the limitations of a coarser particle resolution. In addition, the use of a linear strain-displacement model for the flexible membrane, based on the small deformation assumption, may contribute to discrepancies in stress transfer during large membrane bulging. This could partially explain the fluctuating or diverging stress-strain curves observed at higher CGCs, as the model may underpredict membrane stiffness or boundary constraint effects during deformation. The peak strength in the simulations is slightly overestimated, suggesting that the coarse-graining approach affects the ability of the numerical model to fully replicate the localized particle rearrangements observed in physical tests.

Fig. 8 presents the same comparisons for CGC = 6, where a notable improvement in agreement between experimental and simulated data is observed. The simulated peak stresses align more closely with experimental results, and the fluctuations in stress are significantly reduced. This reduction in oscillatory behavior suggests that increasing the number of particles enables better stress transmission, resulting in a more stable representation of material behavior.

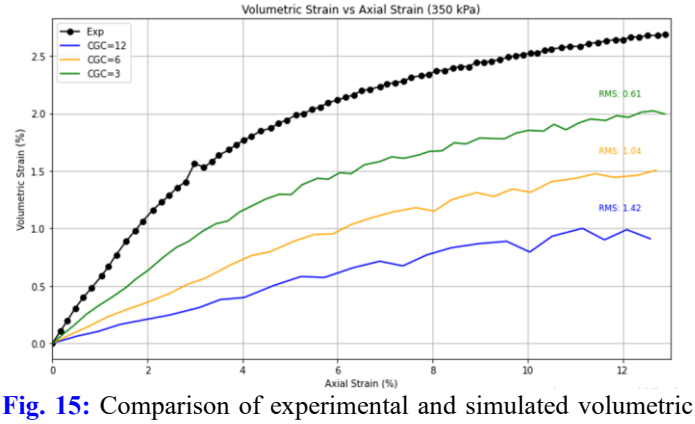

Fig. 15: Comparison of experimental and simulated volumetric strain for 350 kPa at different CGCs.

At CGC = 3, the comparisons, shown in Fig. 9, demonstrate the highest level of agreement with experimental data. The stress-strain response is accurately reproduced across all three confining pressures, with minimal deviations in peak stress and strain behavior. The reduction in oscillations and increased smoothness in the stress-strain curves indicate that a finer particle resolution allows for better energy dissipation and stress redistribution, reducing numerical artifacts. However, despite the improved accuracy, the computational cost associated with CGC = 3 is significantly higher, requiring a careful trade-off between resolution and efficiency.

Examining the microscopic response of the numerical model provides further insight into the observed deviations. The oscillations in stress-strain curves, particularly at higher CGC values, can be attributed to localized force chains that form and break as the material deforms. These force chains, visible in the simulation data, cause intermittent stress drops and peaks, mimicking the granular rearrangements seen in physical experiments but at a coarser resolution. The contact network evolution in the numerical simulations also indicates that for higher CGC values, particles experience larger stress fluctuations due to the reduced number of contacts per unit volume.

A detailed Root Mean Square (RMS) error analysis was conducted to quantify the deviation between experimental and numerical stress-strain responses. The RMS values, displayed in figures confirm that CGC = 3 yields the lowest RMS error, reinforcing its superiority in accuracy. However, as the CGC increases, the RMS error becomes more pronounced, reflecting the increased numerical artifacts associated with fewer particles and reduced stress transmission pathways.

These findings emphasize the necessity of balancing computational efficiency and accuracy in DEM-FEM simulations. While CGC = 12 allows for faster computations, it introduces notable stress fluctuations and minor overestimations of peak stress. On the other hand, CGC = 3 closely replicates the experimental behavior, at the cost of significantly higher computational demand. The choice of CGC must therefore consider the desired trade-off between numerical precision and practical simulation feasibility.

3.2.5 Normalized stress vs axial strain analysis

To evaluate the consistency of the numerical simulations with experimental results, the stress values were normalized by the corresponding confining pressure. This normalization allows for a direct comparison between different stress-strain responses across varying confinement levels, independent of absolute stress magnitudes. Fig. 10 presents the normalized experimental stress-strain behavior for 50 kPa, 200 kPa, and 350 kPa. The experimental data exhibits a clear and consistent trend, where the normalized stress increases rapidly in the early stages of deformation, followed by a stabilization phase. This trend remains largely unaffected by the magnitude of the confining pressure, demonstrating a well-preserved stress-strain relationship across all cases.

To assess the accuracy of the DEM-FEM numerical model, the normalized stress-strain response of the CGC = 3 simulation was compared directly against experimental results (Fig. 11). The results indicate a strong agreement between the experimental and simulated trends, particularly in the initial loading phase, where both curves exhibit similar stress evolution. The numerical model captures the overall shape and trend of the experimental data, confirming that CGC = 3 provides a sufficiently detailed representation of granular interactions for an accurate stress response.

Despite the strong agreement, minor deviations emerge in the post-peak stress behavior, where the simulation exhibits slight over-predictions in normalized stress. This discrepancy is likely due to numerical artifacts inherent in DEM

simulations, particularly related to force chain reconfigurations and boundary interactions. However, the magnitude of these deviations remains small, suggesting that CGC = 3 effectively balances computational efficiency and accuracy.

Overall, the results confirm that the DEM-FEM model, using CGC = 3, successfully replicates the experimental stress-strain trends across different confinement levels. The normalization approach highlights the robustness of the numerical model in capturing essential stress transmission mechanisms within the granular assembly. The findings reinforce the suitability of CGC = 3 for further analyses, ensuring both computational feasibility and high-fidelity representation of real soil behavior.

3.2.6 Volumetric strain vs axial strain comparison

The evolution of volumetric strain in the simulated triaxial tests provides essential insights into the internal mechanics of particle rearrangement and porosity development under axial loading. The DEM-FEM model effectively captures the dilative and contractive tendencies of the granular medium by resolving individual particle interactions and membrane deformations at the micro-scale.

Fig. 12 shows the volumetric strain versus axial strain behavior obtained from the DEM-FEM simulations for three confining pressures (50 kPa, 200 kPa, and 350 kPa) using a CGC of 3. A clear distinction in volumetric response is observed across the different confinement levels. At 50 kPa, the simulated specimen demonstrates an early contractive phase followed by a significant dilative response, closely matching the experimental trend shown in Fig. 5. At 200 kPa, the transition from contraction to dilation occurs more gradually, whereas at 350 kPa, the specimen remains in a contractive state for a more extended period before modest dilation is observed.

The DEM-FEM simulation results of volumetric strain across axial strains are analyzed against experimental data at three confining pressures (50 kPa, 200 kPa, and 350 kPa) for coarse-graining coefficients (CGCs) of 3, 6, and 12 (Fig. 13-15). The comparative assessment reveals crucial differences influenced by the coarse-graining level and confining pressures, offering insight into their root causes.

At 50 kPa confining pressure (Fig. 13), the experimental data exhibit clear initial contractive behavior followed by marked dilation after approximately 3% axial strain, eventually reaching substantial volumetric dilation exceeding 1.5%. In contrast, all CGC simulations significantly underestimate the magnitude of dilation. CGC=3, although closest to the experimental curve (RMS error of 0.44), still noticeably underpredicts dilation, indicating difficulty in capturing particle rearrangement that causes dilation under low confinement. CGC=6 (RMS = 0.69) further diminishes dilation magnitude, and CGC=12 (RMS = 0.80) presents the most severe underestimation, displaying nearly negligible dilation throughout loading. These differences primarily stem from insufficient particle resolution at higher CGCs, failing to accurately represent the granular rearrangements and dilative tendencies observed experimentally at low confining pressure conditions.

At an intermediate 200 kPa confining pressure (Fig. 14), experimental observations demonstrate a moderate contraction initially, transitioning clearly into a dilative regime after approximately 4% axial strain. Simulations at all CGCs deviate significantly from experimental results, especially after reaching peak dilation (~4–5% axial strain). The CGC = 3 case (RMS = 0.28) closely matches initial contraction and early dilation phases but diverges notably beyond 6% axial strain, maintaining a nearly constant volumetric strain rather than reproducing the experimental dilation trend. CGC = 6 (RMS = 0.32) and CGC = 12 (RMS = 0.34) simulations also plateau prematurely, substantially underestimating late-stage dilation. Here, differences are likely caused by limitations in particle-scale modeling resolution and particle rearrangement dynamics, preventing realistic representation of progressive dilation occurring at mid-level confinement.

Under the highest 350 kPa confining pressure (Fig. 15), experimental data display pronounced contractive behavior, continuously increasing volumetric strain up to around 2.5% at approximately 12% axial strain. Simulations systematically underestimate volumetric contraction, with discrepancies increasing significantly at higher CGCs. Specifically, CGC = 3 (RMS = 0.61) moderately follows experimental trends but underestimates the magnitude of contraction notably. CGC = 6 (RMS = 1.04) and CGC = 12 (RMS = 1.42) drastically underestimate volumetric contraction, demonstrating limited sensitivity to high confining pressure conditions. Such stark differences occur because fewer, larger particles at high CGC restrict accurate modeling of particle interactions, diminishing realistic representation of particle packing densification under high pressure.

When comparing across different confining pressures, simulations at lower CGC (CGC = 3) consistently yield the most accurate trends relative to experimental results. However, even this level struggles with accurately modeling large volumetric dilation at low confinement (50 kPa) and significant contraction at high confinement (350 kPa). Higher CGC simulations universally suffer larger discrepancies, indicating that coarse-graining predominantly affects the simulation's capability to replicate granular behavior realistically, especially critical dilative or contractive behaviors directly linked to particle rearrangement.

Overall, these observed differences are primarily attributed to the fundamental limitation imposed by coarse-graining strategies, where increasing the CGC dramatically reduces the particle resolution. Reduced particle counts result in less detailed contact networks, diminished modeling of internal particle interactions, and simplified representations of localized deformation phenomena like bulging and strain localization. Consequently, simulations struggle to capture nuanced volumetric behaviors that depend heavily on

microstructural rearrangements and evolving particle-level interactions.

In conclusion, while DEM-FEM simulations successfully demonstrate the ability to represent general trends in volumetric strain responses across different confinement levels, accuracy greatly depends on the particle resolution provided by lower CGC. To improve predictive reliability in capturing both dilative and contractive granular behavior, careful selection of CGC levels remains crucial, balancing the computational feasibility with required accuracy for practical geotechnical applications.

4. Discussion

This study highlights the potential of the coupled DEM-FEM approach in advancing triaxial testing simulations of granular materials. Although DEM-FEM coupling has been used previously, traditional models often rely on rigid boundaries, simplified contact laws, or coarse mesh–particle interactions that limit fidelity. By integrating a deformable FEM-based membrane, calibrated Hertz–Mindlin contact modeling, and a validated coarse-graining strategy, the present work bridges micro-scale particle interactions and macro-scale deformation behaviors, achieves close agreement with experimental stress–strain responses, and captures micromechanical features such as dilation and shear-band formation. These enhancements greatly improve boundary realism and computational efficiency, offering a robust tool for accurately reproducing complex soil-mechanics phenomena under triaxial loading.

The investigation into coarse-graining strategies was particularly insightful, revealing clear trade-offs between numerical accuracy and computational efficiency. The analyses demonstrated that higher coarse-graining coefficients (*e.g.*, CGC = 12) dramatically reduced computational costs but introduced considerable numerical fluctuations and artifacts, thereby limiting the reliability of simulated stress-strain and volumetric strain responses. Conversely, the lowest coarse-graining coefficient (CGC = 3) yielded highly accurate simulations closely matching experimental observations; however, the computational expense was substantial.

Importantly, the study identifies an optimal compromise at CGC = 6, balancing the demands of accuracy and computational efficiency. This result is especially valuable for practical engineering applications, as it enables efficient simulation of granular materials without significantly sacrificing accuracy. This optimal balance represents a meaningful advancement in the selection criteria for coarse-graining in computational geotechnics.

The normalization analysis further validates the robustness of the simulation framework. Normalized stress-strain data for both experimental and simulation cases converge consistently across all confining pressures, stabilizing at values between 1.3 and 1.4. This consistency underscores the ability of the DEM-FEM framework to preserve the essential mechanics of soil behavior despite varying particle resolutions. However, the normalization data also highlights the impact of coarse-graining on result stability. Simulations with higher CGC values exhibit greater deviations in normalized trends, particularly during the transition from elastic to plastic behavior. These deviations are minimized at lower CGC values, reinforcing the importance of fine particle resolution for capturing critical material responses accurately.

Comparisons with existing literature underscore the novelty of integrating advanced contact models and realistic boundary interactions within a unified DEM-FEM framework. Previous studies frequently relied on simplified rigid boundaries or individual numerical methods, often failing to capture the nuanced interactions that govern granular material behavior under realistic loading conditions. In contrast, the current study clearly illustrates that incorporating flexible membranes and accurate contact mechanics substantially enhances the fidelity of numerical simulations.

Nevertheless, the study acknowledges several limitations. The numerical artifacts at higher coarse-graining levels highlight inherent constraints within DEM simulations, such as sensitivity to particle number and contact distribution. Furthermore, while the flexible membrane integration substantially improved realism, further refinement may be necessary to account for more complex material properties and membrane-soil interactions observed in practical engineering scenarios.

The developed DEM-FEM framework, validated through detailed experimental comparisons, has direct and significant implications for practical engineering. Its ability to accurately replicate soil deformation behaviors such as dilation and strain localization makes it suitable for addressing key geotechnical challenges. For example, it can improve predictions in slope stability analysis by helping engineers assess the potential for landslides based on realistic soil behavior. In foundation engineering, the model can enhance the understanding of settlement patterns and bearing capacity under varying load conditions. Furthermore, the approach is valuable for the design and safety evaluation of earth structures, including embankments, retaining walls, and infrastructure foundations, contributing to their long-term performance and resilience.

Future research should explore adaptive coarse-graining strategies capable of dynamically adjusting particle resolution based on local stress or strain conditions, potentially further optimizing accuracy and efficiency. Additionally, exploring more sophisticated contact models or multi-scale coupling methods could enhance the predictive capability of DEM-FEM frameworks, particularly for diverse granular materials and complex loading scenarios.

In summary, the study substantially advances computational geotechnics by demonstrating the effectiveness and practicality of coupled DEM-FEM modeling. By optimizing coarse-graining strategies and realistically capturing boundary conditions and particle interactions, the research paves the way for more accurate and efficient predictive tools, significantly benefiting geotechnical engineering practices.

4.1 Limitations

While the coupled DEM–FEM framework captures the macro- and micro-mechanical response of dense quartz sand under drained monotonic triaxial compression, its present scope is restricted in several ways. Validation is confined to a single granular soil and loading path, so the model's predictive power for cohesive clays, silts or cyclic stress histories remains untested. Particles are idealized as spheres, neglecting the angularity and fabric anisotropy that can alter strength and dilatancy; future variants will incorporate clumped or polyhedral shapes. The latex membrane is represented by a linear elastic law, whereas large radial bulging may require hyper-elastic or yield formulations to avoid overstiff boundary feedback. Coarse-graining has been benchmarked only up to CGC = 12, and higher ratios amplify stress oscillations; an adaptive, region-refined strategy is being developed to maintain accuracy near shear bands while curbing computational cost elsewhere. Tackling these limitations will extend the framework's generality and practical value across a broader spectrum of geomaterials and engineering scenarios.

5. Conclusion

This study has demonstrated the capability and robustness of the DEM-FEM coupling framework in modeling the mechanical behavior of granular materials under triaxial loading conditions. By systematically varying the CGC, we have explored the trade-offs between computational efficiency, accuracy, and stability in numerical simulations.

The findings reveal that while simulations with higher CGC values (*e.g.*, CGC = 12) are computationally efficient, they introduce significant numerical artifacts, such as amplified fluctuations in stress-s+train behavior. Conversely, lower CGC values (*e.g.*, CGC = 3) minimize these artifacts and closely replicate experimental results, albeit at the cost of increased computational resources and simulation time. CGC = 6 emerges as a practical compromise, balancing computational efficiency with adequate accuracy for most engineering and research applications.

The normalization analysis further validates the simulation framework, demonstrating consistent convergence of stress-strain data across all confining pressures and CGC values. This convergence underscores the ability of the DEM-FEM framework to preserve the fundamental mechanics of granular materials despite variations in particle resolution.

In addition to providing insights into coarse-graining strategies, this study highlights the importance of parameter selection, including Young's modulus and friction coefficients, in achieving reliable simulation outcomes. The results emphasize that coarse-graining should be carefully tailored to the specific requirements of a given study, considering factors such as computational resources, desired accuracy, and the complexity of material behavior.

Future research directions include the development of advanced coarse-graining techniques to reduce numerical artifacts and improve the fidelity of high-CGC simulations. Investigating the influence of particle shape, contact laws, and boundary conditions on simulation accuracy will also enhance the applicability of the DEM-FEM framework in modeling complex granular systems.

In conclusion, this study provides a comprehensive evaluation of coarse-graining strategies within the DEM-FEM framework, offering valuable guidance for selecting appropriate modeling approaches in the analysis of granular materials. The findings contribute to the advancement of computational tools for soil mechanics and related fields, supporting more efficient and accurate simulations of complex material behaviors.

Acknowledgements

This research was supported by the Ministry of Science and Higher Education of the Republic of Kazakhstan, grant No. AP19678197 ("Integrating Physics-Informed Neural Network, Bayesian and Convolutional Neural Networks for early breast cancer detection using thermography") and by Nazarbayev University FDCR grant No. 20122022FD4126.

Conflict of Interest

The authors declare that the research was conducted in the absence of any commercial or financial relationships that could be construed as a potential conflict of interest.

Data Availability Statement

The datasets generated and analyzed for this study can be found in the Triaxial Test DEM-FEM Simulation Repository at https://github.com/SayakovOE/Triaxial-test-DEM-FEM-simulation.git. The repository contains the source code, simulation scripts, and validation datasets used in this research.

Supporting Information

Applicable.

CRediT Statement

Olzhas Sayakov and **Michael Yong Zhao:** conceptualization. **Olzhas Sayakov**, **Sonny Irawan** and **Bakhtiyar Kalzhan:** investigation. **Minh Nguyen** and **Michael Yong Zhao:** methodology and formal analysis. **Michael Yong Zhao**, **Dongming Wei** and **Sonny Irawan:** funding acquisition. **Olzhas Sayakov** and **Bakhtiyar Kalzhan:** software development. **Olzhas Sayakov**, **Kamila Batkuldinova** and **Ainash Shabdirova:** validation. **Ainash Shabdirova:** conducted experiment. **Olzhas Sayakov**, **Bakhtiyar Kalzhan** and **Kamila Batkuldinova:** visualization. **Olzhas Sayakov** and **Michael Yong Zhao:** writing – original draft. **Michael Yong Zhao**, **Sonny Irawan**, **Dongming Wei** and **Minh Nguyen:** review, editing, and final approval.

References

[1] F. Faris, F. Wang, Investigation of the initiation mechanism of an earthquake- induced landslide during rainfall: a case study of the Tandikat landslide, West Sumatra, Indonesia,

Geoenvironmental Disasters, 2014, **1**, 4, doi: 10.1186/s40677-014-0004-3.

[2] M. F. Ahlinhan, E. Houehanou, M. B. Koube, V. Doko, Q. Alaye, N. Sungura, E. Adjovi, Experiments and 3D DEM of triaxial compression tests under special consideration of particle stiffness, *Geomaterials*, 2018, **8**, 39-62, doi: 10.4236/gm.2018.84004.

[3] A. S. Abood, M. Y. Fattah, A. Al-Adili, Assessment of shear strength characteristics of the unsaturated gypseous soil at various saturation degrees, *Cogent Engineering*, 2023, **10**, 2283303, doi: 10.1080/23311916.2023.2283303.

[4] X. Yang, S. Liang, Z. Hou, D. Feng, Y. Xiao, S. Zhou, Experimental study on strength of polypropylene fiber reinforced cemented silt soil, *Applied Sciences*, 2022, **12**, 8318, doi: 10.3390/app12168318.

[5] T. Yoshikawa, T. Noda, Triaxial test on water absorption compression of unsaturated soil and its soil-water-air-coupled elastoplastic finite deformation analysis, *Soils and Foundations*, 2020, **60**, 1151-1170, doi: 10.1016/j.sandf.2020.06.010.

[6] J. Chu, D. Wanatowski, Effect of loading mode on strain softening and instability behavior of sand in plane-strain tests, *Journal of Geotechnical and Geoenvironmental Engineering*, 2009, **135**, 108-120, doi: 10.1061/(asce)1090-0241(2009)135:1(108).

[7] M. Safdar, T. Newson, F. Shah, Consolidated drained (CID) behavior of fibre reinforced cemented Toyoura sand in triaxial loading conditions, *International Journal of Geo-Engineering*, 2021, **12**, 27, doi: 10.1186/s40703-021-00165-0.

[8] M. D. Bolton, Discussion: the strength and dilatancy of sands, *Géotechnique*, 1987, **37**, 517, doi: 10.1680/geot.1987.37.4.517.

[9] N. Della, H. Missoum, A. Arab, M. Belkhatir, Experimental study of the overconsolidation and saturation effects on the mechanical characteristics and residual strength of Chlef river sandy soil, *Periodica Polytechnica Civil Engineering*, 2010, **54**, 107, doi: 10.3311/pp.ci.2010-2.06.

[10] M. Hassanlourad, H. Salehzadeh, H. Shahnazari, Mechanical properties of ungrouted and grouted carbonate sands, *International Journal of Geotechnical Engineering*, 2010, **4**, 507-516, doi: 10.3328/ijge.2010.04.04.507-516.

[11] S. Yimsiri, K. Soga, DEM analysis of soil fabric effects on behaviour of sand, *Géotechnique*, 2010, **60**, 483-495, doi: 10.1680/geot.2010.60.6.483.

[12] E. Salvatore, R. L. Spacagna, E. Andò, M. Ochmanski, Geostatistical analysis of strain localization in triaxial tests on sand, *Géotechnique Letters*, 2019, **9**, 334-339, doi: 10.1680/jgele.18.00228.

[13] A. I. Theocharis, E. Vairaktaris, Y. F. Dafalias, A. G. Papadimitriou, Necessary and sufficient conditions for reaching and maintaining critical state, *International Journal for Numerical and Analytical Methods in Geomechanics*, 2019, **43**, 2041-2055, doi: 10.1002/nag.2943.

[14] Y. Qin, C. Liu, X. Zhang, X. Wang, B. Shi, Y. Wang, S. Deng, A three-dimensional discrete element model of triaxial tests based on a new flexible membrane boundary, *Scientific Reports*, 2021, **11**, 4753, doi: 10.1038/s41598-021-84224-7.

[15] T. Yang, W. Zheng, H. Zhang, X. Yue, Triaxial shear analysis using discrete element methods for sandy soil with an improved flexible membrane boundary, *Sustainability*, 2023, **15**, 12911, doi: 10.3390/su151712911.

[16] G. Ma, W. Zhou, X.-L. Chang, W. Yuan, Combined FEM/DEM modeling of triaxial compression tests for rockfills with polyhedral particles, *International Journal of Geomechanics*, 2014, **14**, 04014014, doi: 10.1061/(asce)gm.1943-5622.0000372.

[17] T. Qu, Y. T. Feng, Y. Wang, M. Wang, Discrete element modelling of flexible membrane boundaries for triaxial tests, *Computers and Geotechnics*, 2019, **115**, 103154, doi: 10.1016/j.compgeo.2019.103154.

[18] T. Mohamed, J. Duriez, G. Veylon, L. Peyras, Flexible membrane boundary condition DEM-FEM for drained and undrained monotonic and cyclic triaxial tests, *Granular Matter*, 2024, **26**, 94, doi: 10.1007/s10035-024-01462-y.

[19] S. Huang, Y. Qian, Y. Shan, Effect of flexible membrane in large-scale triaxial test DEM simulations, *Construction and Building Materials*, 2023, **370**, 130608, doi: 10.1016/j.conbuildmat.2023.130608.

[20] J. Desrues, A. Argilaga, D. Caillerie, G. Combe, T. K. Nguyen, V. Richefeu, S. Dal Pont, From discrete to continuum modelling of boundary value problems in geomechanics: An integrated FEM-DEM approach, *International Journal for Numerical and Analytical Methods in Geomechanics*, 2019, **43**, 919-955, doi: 10.1002/nag.2914.

[21] M. Wu, Y. Fan, J. Wang, Z.-Y. Yin, Modeling a flexible membrane for triaxial tests with coupled FDM–DEM: considering realistic particle shape effects, *International Journal of Geomechanics*, 2024, **24**, 04024155, doi: 10.1061/ijgnai.gmeng-9789.

[22] M. Michael, B. Peters, and F. Vogel, "An Efficient 3D FEM - DEM Coupling for Granular Matter Applications," in *NAFEMS European Conference on Coupled MBS-FE Applications*, 2013.

[23] W. Liu, Q. Su, M. Fang, J. Zhang, W. Zhang, Z. Yu, Parameters calibration of discrete element model for corn straw cutting based on hertz-mindlin with bonding, *Applied Sciences*, 2023, **13**, 1156, doi: 10.3390/app13021156.

[24] S. Mudarisov, I. Farkhutdinov, R. Khamaletdinov, E. Khasanov, A. Mukhametdinov, Evaluation of the significance of the contact model particle parameters in the modelling of wet soils by the discrete element method, *Soil and Tillage Research*, 2022, **215**, 105228, doi: 10.1016/j.still.2021.105228.

[25] Y. Wang, J.-Y. Nie, S. Zhao, H. Wang, A coupled FEM-DEM study on mechanical behaviors of granular soils considering particle breakage, *Computers and Geotechnics*, 2023, **160**, 105529, doi: 10.1016/j.compgeo.2023.105529.

[26] A. Di Renzo, E. Napolitano, F. Di Maio, Coarse-grain DEM modelling in fluidized bed simulation: a review, *Processes*, 2021, **9**, 279, doi: 10.3390/pr9020279.

[27] B. Zhang, Y. Huang, T. Zhao, Comparison of coarse graining DEM models based on exact scaling laws, *Computer Modeling in Engineering & Sciences*, 2021, **127**, 1133-1150, doi: 10.32604/cmes.2021.016018.

[28] D. Kazidenov, F. Khamitov, Y. Amanbek, Coarse-graining of

CFD-DEM for simulation of sand production in the modified cohesive contact model, *Gas Science and Engineering*, 2023, **113**, 204976, doi: 10.1016/j.jgsce.2023.204976.
[29] D. Queteschiner, T. Lichtenegger, S. Schneiderbauer, Stefan Pirker CD Laboratory for Multi-Scale Modelling of Processes, J. Linz, Austria, D. O. P. F. Modelling, L. I. O. Technology, Adaptive coarse-graining for large-scale DEM simulations, *ArXiv: Computational Physics*, 2018
[30] Y. Wang, J.-Y. Nie, S. Zhao, H. Wang, A coupled FEM-DEM study on mechanical behaviors of granular soils considering particle breakage, *Computers and Geotechnics*, 2023, **160**, 105529, doi: 10.1016/j.compgeo.2023.105529.
[31] R. M. Færgestad, J. K. Holmen, T. Berstad, T. Cardone, K. A. Ford, T. Børvik, Coupled finite element-discrete element method (FEM/DEM) for modelling hypervelocity impacts, *Acta Astronautica*, 2023, **203**, 296-307, doi: 10.1016/j.actaastro.2022.11.026.
[32] Y. Peng, Y. Tan, L. Qu, Micromechanical analysis of the suction bucket-granular soil interactions under the pull action of anchor lines: Embedded length effect, *Ocean Engineering*, 2024, **291**, 116443, doi: 10.1016/j.oceaneng.2023.116443.
[33] H. Zhang, L. Zhang, H. Zhang, J. Wu, X. An, D. Yang, Fibre bridging and nozzle clogging in 3D printing of discontinuous carbon fibre-reinforced polymer composites: coupled CFD-DEM modelling, *The International Journal of Advanced Manufacturing Technology*, 2021, **117**, 3549-3562, doi: 10.1007/s00170-021-07913-7.
[34] S. Zhao, T. M. Evans, X. Zhou, Effects of curvature-related DEM contact model on the macro- and micro-mechanical behaviours of granular soils, *Géotechnique*, 2018, **68**, 1085-1098, doi: 10.1680/jgeot.17.p.158.
[35] J. Shen, H. Wang, B. Zhou, G. Hu, X. Zhang, B. Yang, Investigation of the effect of microbial-induced calcite precipitation treatment on bio-cemented calcareous sands using discrete element method, *Computers and Geotechnics*, 2023, **158**, 105365, doi: 10.1016/j.compgeo.2023.105365.
[36] P. Yang, E. Kavazanjian, N. Neithalath, DEM simulations on the influence of carbonate precipitation on liquefaction mitigation of sand, *Computers and Geotechnics*, 2023, **162**, 105681, doi: 10.1016/j.compgeo.2023.105681.
[37] A. Munjiza and O. Mahabadi, "Numerical modelling of a triaxial test using the combined-finite discrete element method," *Geomechanics Research Group, Lassonde Institute, Civil Engineering Department, University of Toronto, ON, Canada*. Accessed: Apr. 18, 2025. Available: https://www.academia.edu/20289751/5_Numerical_modelling_of_a_triaxial_test_using_the_combined_finite_discrete_element_method
[38] T. Mohamed, J. Duriez, G. Veylon, L. Peyras, Flexible membrane boundary condition DEM-FEM for drained and undrained monotonic and cyclic triaxial tests, *Granular Matter*, 2024, **26**, 94, doi: 10.1007/s10035-024-01462-y.